ACS APPLIED MATERIALS & INTERFACES

Research Article

Cite This: ACS Appl. Mater. Interfaces 2019, 11, 25445−25456

www.acsami.org

Superhydrophobic Polyurethane Foam Coated with Polysiloxane-Modified Clay Nanotubes for Efficient and Recyclable Oil Absorption

Fan Wu,[†] Kylene Pickett,[‡] Abhishek Panchal,[‡] Mingxian Liu,*[,†] and Yuri Lvov*[,‡,§]

[†]Department of Materials Science and Engineering, Jinan University, Guangzhou 510632, China

[‡]Institute for Micromanufacturing, Louisiana Tech University, Ruston, Louisiana 71270, United States

[§]Theoretical Physics & Applied Mathematics Department, Ural Federal University, Ekaterinburg 620002, Russia

Supporting Information

ABSTRACT: Superhydrophobic polyurethane foam (PUF) is prepared by surface coating of halloysite nanotubes. The nanotubes were first modified by surface grafting with hexadecyltrimethoxysilane, followed by assembly on the PUF by dip coating. This treatment makes the water contact angle of the modified PUF higher than 150°. The modified foam has a highly selective absorption of oils and organic solvents. The absorption ratios of the modified PUF for chloroform and dichloroethane reached 104 and 74, respectively. Such superhydrophobic foam can maintain the oil absorption performance even after 10 absorption−squeezing cycles, demonstrating good recyclability. The modified foam can pick up oil or organic solvent continuously and quickly from water's surface. This hydrophobic nanotube coating also enhances the flame retardancy of the PUF, and the modified foam will extinguish itself maintaining its integrity. The preparation method for hydrophobic and flame-retardant PUF by coating with natural clay nanotubes is a simple process and promises scalable applications in oil−water separation.

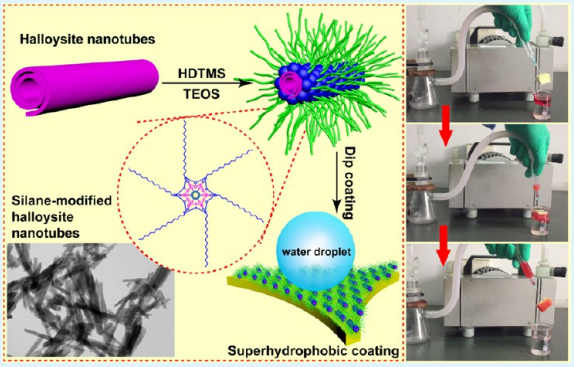

KEYWORDS: *halloysite nanotubes, superhydrophobic, oil absorption, polyurethane foam, surface modification*

1. INTRODUCTION

The ongoing soil and sea pollution by oil demands new and efficient solutions.[1,2] Oil spills during exploration, production, refining, and transportation are difficult to control, which has catastrophic effects on the environment.[3,4] Oil pollution poses a huge threat to seabirds and other marine wildlife.[5] Leaked oil can accumulate in the organs of fish and shellfish, which are consumed by people, and can contaminate groundwater.[6] Oil−water separation materials to filter or absorb the leaked oil is an effective and practical way to solve this problem. Other methods (e.g., mechanical recovery, dispersant, and direct combustion) are time-consuming and labor-intensive and may cause secondary pollution (e.g., using detergent emulsifications).[7,8] Current oil−water separation materials mainly include metal mesh, textile/fabric, and polymer membranes.[9−12] Other materials include powder minerals and synthetic three-dimensional (3D) porous absorbents that are less expensive and quicker processes.[13−15]

Polyurethane foam (PUF) is a cheap and commercially available porous absorbent material.[16−18] It is widely used due to its low density, good elasticity, resistance to organic solvents, and high absorption ability.[19−21] However, PUF absorbs water, oil, and organic solvents at the same time, without selectivity.[22,23] It is very important to improve its water rejection and oil absorption ability. Materials with low surface free energy are often hydrophobic.[24,25] However, a superhydrophobic surface cannot be obtained by only reducing the free energy; surface roughness is also necessary. For example, electrospinning a self-assembly allows for the preparation of a monolithic silica foam that is useful for oil−water separation. This is due to its superhydrophobic/superlipophilic properties after the polydimethylsiloxane coating.[26] In another approach, one-step ultrasonic dip-coating method gives a superhydrophobic sepiolite layer onto the surface of PUF. This foam is capable of rapid and selective absorption of oils and nonpolar solvents.[27] A TiO_2/polyurethane composite modified with tetradecylamine amidated graphene oxide also resulted in a superhydrophobic foam for oil spill cleanup.[28] However, the above superhydrophobic foams have low reusability, complicated manufacturing process, and cannot be applied in a large scale.

Halloysite nanotubes (HNTs) of 50 nm diameter are a natural, tubular clay with a specific surface area of 60−70 m^2/g, and adjustable surface chemistry.[29] The nanotube's outer surface is rich in Si-OH, and its inner lumen is rich in Al-OH groups, which makes it easy to modify through a silanization

Received: May 8, 2019
Accepted: June 18, 2019
Published: June 18, 2019

DOI: 10.1021/acsami.9b08023
ACS Appl. Mater. Interfaces 2019, 11, 25445−25456

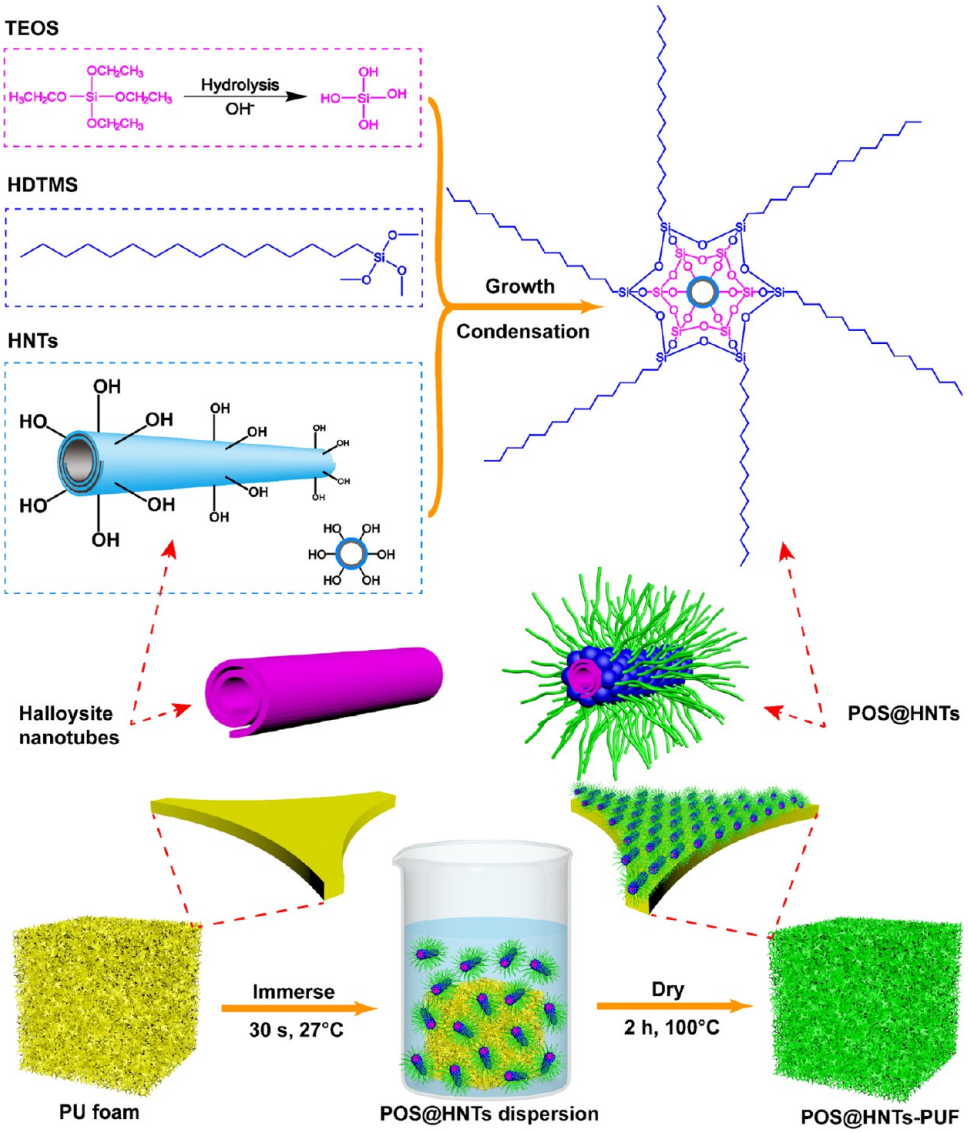

Figure 1. Preparation and reaction mechanism of the superhydrophobic POS@HNTs coated polyurethane foam.

process.[30−32] This nanoclay has many advantages: availability without the need for exfoliation, a high aspect ratio, thermal stability up to 1200 °C, good mechanical strength, well-developed pore structure, and satisfactory water-dispersion stability, allowing for a variety of surface modifications.[33] HNT-coated 3D printed poly(lactic acid) patterns can be used to direct human mesenchymal stem cell orientation.[34] Layer-by-layer nanocoating containing branched polyethyleneimine, polyacrylic acid, and HNTs can effectively reduce PUF flammability.[35] HNT-based poly(methyl methacrylate)/polystyrene nanocomposite coating has improved thermal stability and scratch resistance, and it can be used in glass for automotive and architectural applications.[36]

Raw HNTs are a hydrophilic material with a surface ζ-potential of ca −30 mV. This means it has a low oil absorption rate.[37] Therefore, the hydrophobic modification of HNTs is important for its oil absorption enhancement. Hydrolysis and condensation reactions between hydroxyl groups on nanoparticles and alkoxysilanes are commonly used for hydrophobic modification of materials.[38−41] In our previous work, the hydrophobic HNTs were obtained by the condensation reaction of hexadecyltrimethoxysilane (HDTMS) with tetraethoxysilane (TEOS).[42] Since the long-chain alkyl group reduces the surface free energy and the tubes have a nanoscale roughness, the HNT's surface hydrophobicity is greatly improved. However, there has not yet been a simple and effective preparation method of polymer foam coated with hydrophobic HNTs.

Here, we present a simple and effective strategy for novel oil−water separation foam using polysiloxane-modified halloysite nanotube (POS@HNT) dip-coating process. Superhydrophobic HNT powder was obtained by the grafting of HDTMS and TEOS. POS@HNT has rough micro/nanoscale structures and a low surface free energy, making the modified foam superhydrophobic. This foam can continuously, effectively, and quickly separate the oil or organic solvent from the water. The superhydrophobic PUF also has improved flame retardancy, an important feature for large-scale applications in sea oil spill cleanup.

2. RESULTS AND DISCUSSION

2.1. Surface Modification of Halloysite. The synthesis of POS@HNTs and the dip-coating process of PUF are illustrated in Figure 1. HNTs were first uniformly dispersed in

DOI: 10.1021/acsami.9b08023
ACS Appl. Mater. Interfaces 2019, 11, 25445−25456

an ethanol/ammonium hydroxide mixed solution. Next, TEOS was hydrolyzed under alkaline conditions to form orthosilicic acid. After that, orthosilicic acid chemically reacted with the hydroxyl group on the tube's surface and was grafted as a coupling agent. Finally, HDTMS was hydrolyzed and condensed to anchor on the nanotubes imparting hydrophobic properties to the HNT with their 16-carbon-long alkane chain. Commercially purchased PUF was first washed and dried. Then, POS@HNTs dispersed in absolute ethanol were assembled on PUF via a dip-coating process. The main role of TEOS is as a coupling agent to improve the hydrolytic condensation of HDTMS on the surface of HNTs.[43] Water contact angle of HDTMS-modified HNTs (HDTMS@HNTs) is only 142.5° (Supporting Information, Figure S1).

The surface morphology of POS@HNTs was first observed with scanning and transmission electron microscopy (SEM and TEM respectively). Figure 2A,B compares the morphology of the nanotubes before and after modification. Raw HNTs show a typical tubular morphology with a smooth surface. However, after surface modification, the diameter of the POS@HNTs becomes larger and the surface becomes rough due to the grafting of a layer of polysiloxane. The results of TEM indicate that the diameter of POS@HNTs is in 60−90 nm after surface

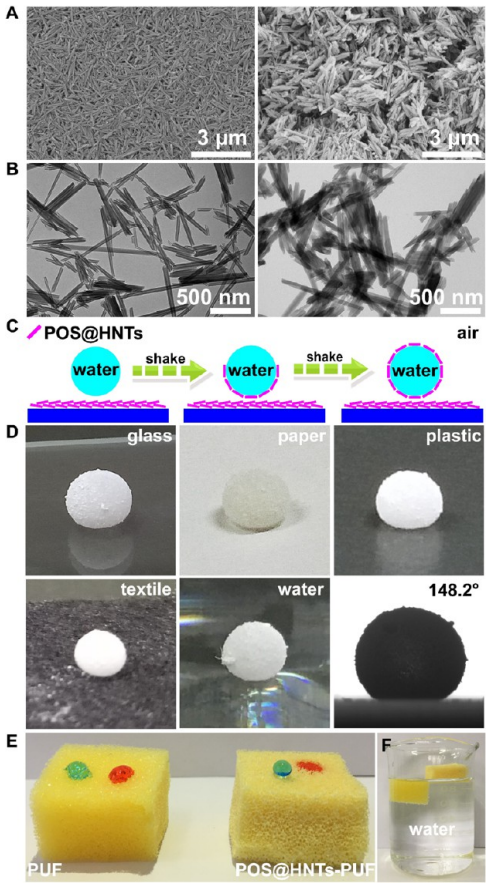

Figure 2. SEM and TEM images of HNTs and POS@HNTs (A, B). Formation process of hydrophobic halloysite marble (C). Hydrophobic halloysite marble located on various surfaces (D). Wettability of original PUF and modified POS@HNT-PUF. Photograph of water and oil on the surface of the PUF and POS@HNT-PUF (water (blue) and oil (red) are colored with methylene blue and Sudan III, respectively) (E). Modified POS@HNT-PUF floats on the water while original PUF sinks in the water (F).

modification. The cavity of the modified nanotubes was partially filled with POS because the inner surface of HNTs also has hydroxyl groups.

Interestingly, when water was dropped onto the hydrophobized POS@HNT powder, a halloysite-coated marble was formed (Figure 2C). The marble has a layer of POS@HNTs on its outer surface. The marble demonstrates hydrophobicity while "sitting" on glass, paper, polyethylene, textile, and water (Figure 2D) (Supporting Information, Video SV1). The contact angle of this hydrophobic halloysite marble on the glass is ca. 148°. The POS@HNT marbles exhibit hydrophobic properties due to the surface nanoroughness and the low surface energy of the acetyl chains outside the tube. We expected a similar synergy in superhydrophobicity with polyurethane when coated with the same nanotubes.

Figure 2E shows the wetting properties of raw and halloysite-coated PUF (POS@HNT-PUF). Hydrophobic PUF was obtained by immersing the PUF in a dispersion of POS@HNTs and a subsequent drying of the samples. We compared the foam's behavior in its original hydrophilic and modified lipophilic states. After the oil droplet touches the modified foam, it spreads rapidly on POS@HNT-PUF and is completely absorbed within 1 s. The modified POS@HNT-PUF exhibits water rejection with a low sliding angle (Supporting Information, Video SV2). When soaking the two foams in deionized (DI) water, the original raw PUF sinks, while POS@HNT-PUF floats on the water (Figure 2F). These results indicate that hydrophobized halloysite can be used as a coating to create lipophilic surfaces.

2.2. Morphology and Composition of the Superhydrophobic Foam. Commercial PUF materials are relatively fragile, so mild experimental conditions for coating were applied. The hydrophobic halloysite layer was uniformly distributed on the foam's surface by dipping. With the increases in suspension concentration, the color of POS@HNT-PUF becomes lighter (Figure 3A). The white hydrophobic halloysite layer attenuates the original yellow color of the polyurethane. The adhesion between POS@HNTs and PUF was good since very little powder peeled off from the foam during use, and this is like the situation with the marbles when self-assembled halloysite interlayers to stabilize the coating. The POS@HNTs are self-assembled on the PUF surface via physical interactions such as hydrogen bonding and van der Waals forces. The estimated thickness of the POS@HNT layer on PUF is 100−800 nm much more than a monolayer. The POS@HNT ethanol dispersion was used to coat the PUF surface. In the work of the silanized HNT assembly on hair, it was also found that the binding is predominantly due to van der Waals forces as the hydroxyl centers have been shielded by the aliphatic group.[44]

Polarized optical microscope images of PUF and POS@HNT-PUF show that the unmodified foam has an open-cell structure, and the pore walls are smooth and uniform with similar skeleton cell sizes (Figure 3B). The skeleton of original PUF is a transparent reticular fiber structure and it becomes whitish after HNT coating. With a higher concentration of hydrophobic halloysite in suspension, the coating thickness increases. The PUF coated with hydrophobic clay nanotubes absorbs oil and repels water, which is prospective for oil−water separation devices.[45]

The introduction of nanocoating affects the pore size and shape of the foam, which also changes the density of the foam and the pore morphology.[46] SEM was used to analyze the

DOI: 10.1021/acsami.9b08023
ACS Appl. Mater. Interfaces 2019, 11, 25445−25456

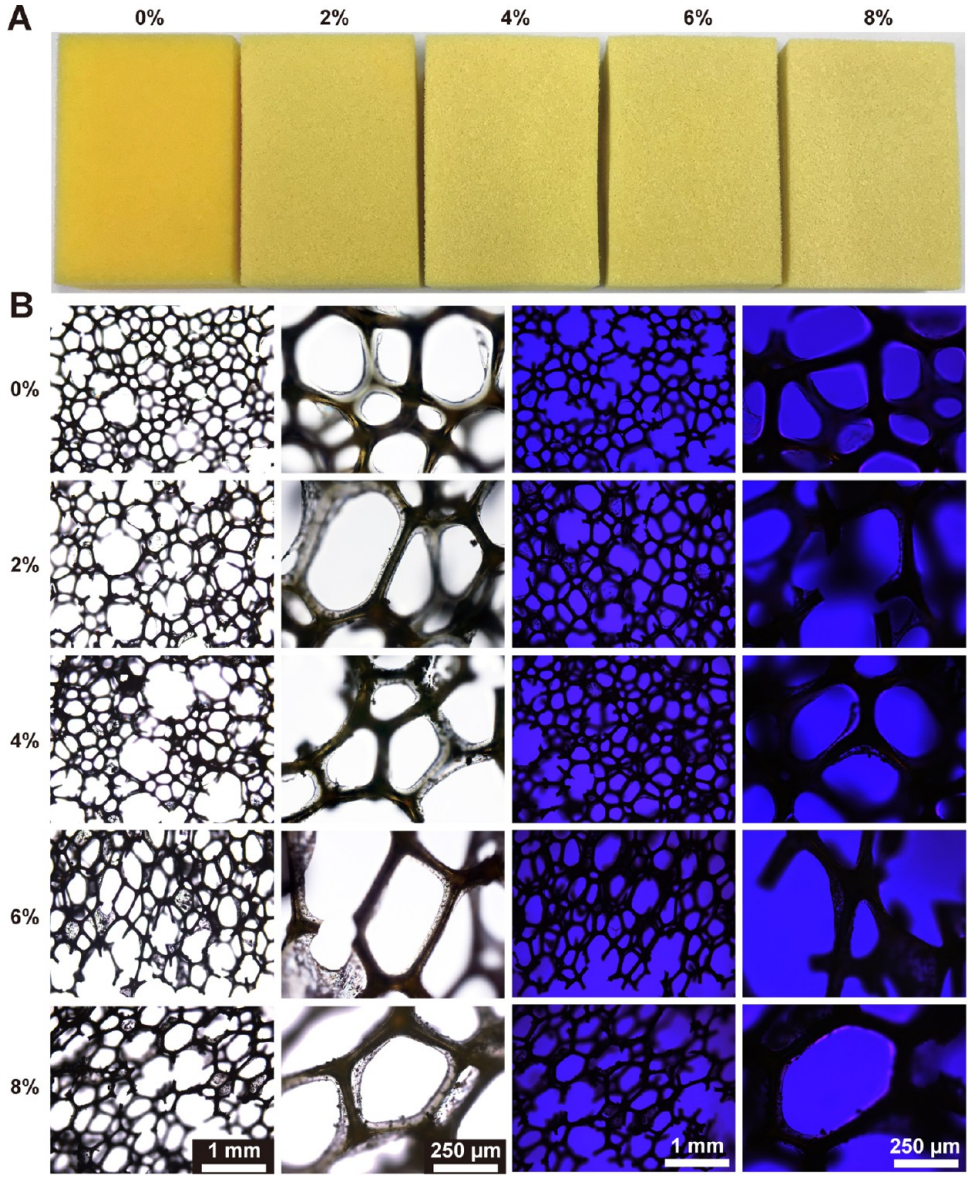

Figure 3. Photographs of original PUF and modified POS@HNT-PUF (size 95 × 65 × 22 cm^3) (A). Polarized optical microscope images of PUF and POS@HNT-PUF at different magnifications (the left two columns, white light; the right two columns: polarized light with the sensitive tint plate insertion) (B).

surface morphology changes before and after halloysite coating (Figure 4). The surface of original raw PUF is clean and smooth. In contrast, the surface of modified POS@HNT-PUF is rough and covered with nanotubes, as seen at a higher magnification. There are no significant changes in the pore size after coating, staying within 200−500 μm. Modified POS@HNTs-PUF maintains a good open-cell structure. This means that the POS@HNT dip-coating process is gentle and does not damage the original pore structure of the foam. The open-cell structure of the foam is a necessary condition for the oil and organic solvent to enter inside the foam, which maximizes oil absorption.[47]

The surface topography of the pore wall was characterized by high-magnification SEM images (Figure 5A). The nanotubes are distributed on the surface of the foam skeleton, and the original structure of the pores is not destroyed during the coating process. POS@HNTs are attached on the foam so that the surface of the modified PUF becomes rough. The halloysite coating has agglomerates, which constitute the micro−nano organization of POS@HNT-PUF. This submicron roughness of the pore surface is beneficial for increasing the hydrophobicity of the foam. Figure 5B,C compares the X-ray photoelectron spectra (XPS) of original PUF and modified 8% POS@HNT-PUF. Significant differences in the elemental composition of the foam were found before and after modification. An increase in the oxygen and aluminum concentrations in modified PUF indicates the successful coating with POS-HNTs. The concentrations of aluminum, silicon, and oxygen in the modified foam increased from 0.76 to 2.05%, from 5.81 to 7.65%, and from 24.54 to 26.7%, respectively. The peak strength of Al 2p and Si 2p increases significantly, which also suggests the adhesion of aluminosilicate HNTs. The presence of Si 2p photoelectron peaks in the high-resolution spectra of commercial PUF can be attributed to the use of silicon-containing compounds (silanes) as a surfactant in the fabrication of the commercial PUF.[35,48]

DOI: 10.1021/acsami.9b08023
ACS Appl. Mater. Interfaces 2019, 11, 25445−25456

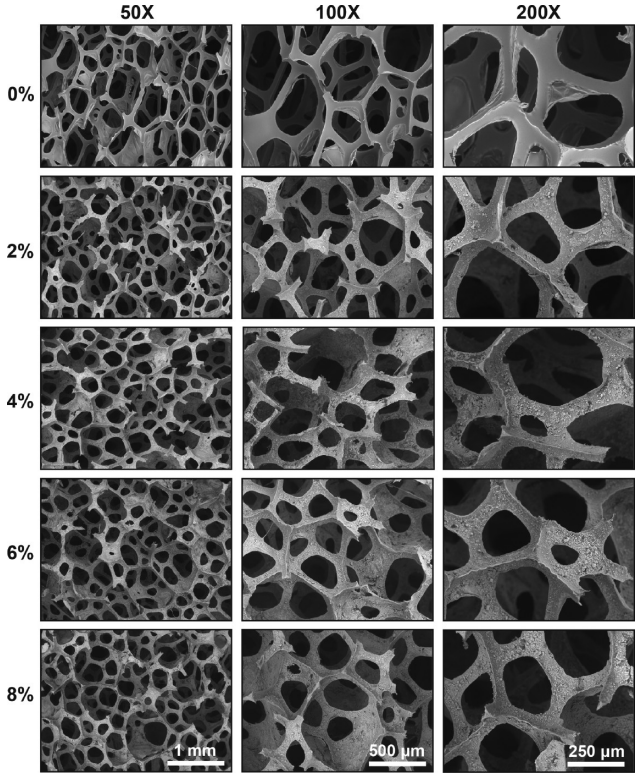

Figure 4. SEM images of PUF and POS@HNT-PUF in different magnifications.

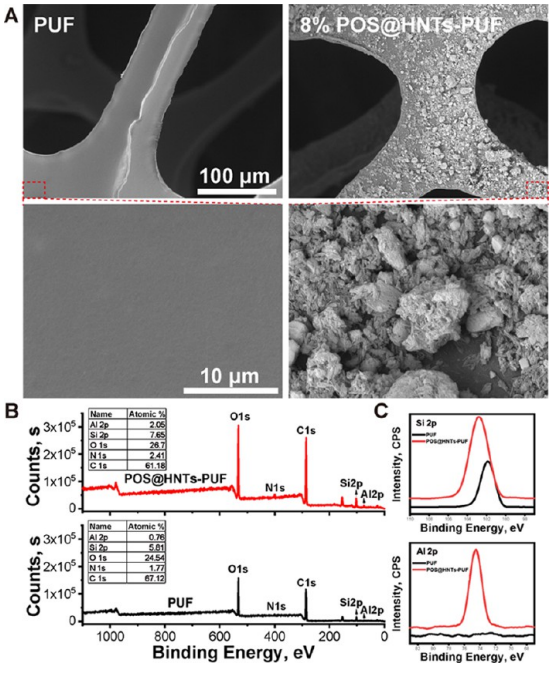

Figure 5. SEM images of PUF and POS@HNT-PUF surfaces (A); scale bar is the same for left and right images. XPS spectra of PUF and POS@HNT-PUF (B and C).

Modified POS@HNT-PUF was further characterized by X-ray diffraction (XRD) and Fourier transform infrared (FTIR) spectroscopy, Figure 6. The XRD patterns of HNTs, POS@HNTs, and all modified PUF samples are shown in Figure 6A. The raw HNTs show Bragg peaks at 2θ of 11.7, 20.1, 24.7, and 35° assigned to (001), (020, 110), (002), and (200, 130) crystalline planes. Consistent with the previous literature, the diffraction peak of halloysite does not change significantly after silanization, indicating that no crystal phase changes occur during the grafting process.[42,49] For raw PUF, an amorphous diffraction peak was observed at 2θ of 21°, which follows the literature.[50] Foams with different nanotube concentrations have similar XRD patterns with enhanced peak intensities for higher halloysite concentrations. In addition, the diffraction peaks at 20.1 and 24.7° of the modified foam slightly deviated from the location of the peak of the raw POS@HNTs.

The FTIR peaks at 3695 and 3620 cm^{-1} are attributed to the stretching vibration of the inner-surface hydroxyls and the inner hydroxyls.[51] The asymmetric tensile vibration absorption band of Si−O−Si is near 1030 cm^{-1}, and the single Al-OH bending band is located at 910 cm^{-1}.[52] POS@HNTs showed two new peaks at 2920 and 2850 cm^{-1}, which can be attributed to the tensile vibration of the aliphatic CH groups.[49] These peaks also appear in the POS@HNT-PUF, indicating that hydrophobic halloysite is successfully coated on the foam. The intensity of these peaks increases with the concentration of the POS@HNT suspension.

2.3. Properties of the Superhydrophobic Foam. The absorption capacity of the polymer foam is directly related to its density and porosity.[53] Figure 7A,B compares the density and porosity of the foams with different POS@HNT concentrations. The density of the original raw PUF is 22.6 mg/cm^3, while the density of the modified foam increases with the halloysite dispersion concentration. This indicates that more POS@HNTs are attached to the surface of the foam during dip coating. At the same time, the porosity of the POS@HNT-PUF slightly decreases. The porosity of the raw foam is 87.6%, while the porosity of the foam coated with 8% POS@HNT decreases to 50.1%. Therefore, to achieve the highest absorption capacity, a moderate concentration of POS@HNT-PUF should be used. Generally, a decrease in porosity results in a more compact structure, leading to an increase in the mechanical strength. In addition, the inorganic HNTs have high strength and Young's modulus, reinforcing polymers. As expected, the compressive properties of the POS@HNT-PUF are increased by incorporation of POS@HNTs (Supporting Information, Figure S2). The thermal stability of the different foams was analyzed by thermogravimetric analysis (TGA) (Figure 7C,D). Since the halloysite contains absorbed water and hydroxyl groups on their surfaces, its weight loss in pristine form is 16.9 ± 0.2%. Due to the decomposition of grafted silane, the total weight loss of POS@HNTs is higher and equals 30.1 ± 0.2% and their difference of 15.9 ± 0.4% may be attributed to the grafted POS.

Uncoated foam almost completely decomposed in the temperature range of 350−450 °C, and the residual weight at 700 °C is 0.7%. In contrast, when the foam is coated with POS@HNTs, the residual weights with 2, 4, 6, and 8% POS@HNTs at 700 °C are 16.2, 31.4, 43.0, and 56.1%, respectively, while the calculated weight ratios of hydrophobized halloysite coated on the foam are 22.1, 44.0, 60.6, and 79.3%, respectively. At a 2% POS@HNT concentration, both the initial degradation temperature and the second degradation temperature of PUF increases (Figure 7D). However, at higher concentrations, these two temperatures decreasesd. The accelerated degradation behavior of polymers with clay was indicated previously, which could be due to the presence of chromophores and traces of iron in halloysite.[54,55]

DOI: 10.1021/acsami.9b08023
ACS Appl. Mater. Interfaces 2019, 11, 25445−25456

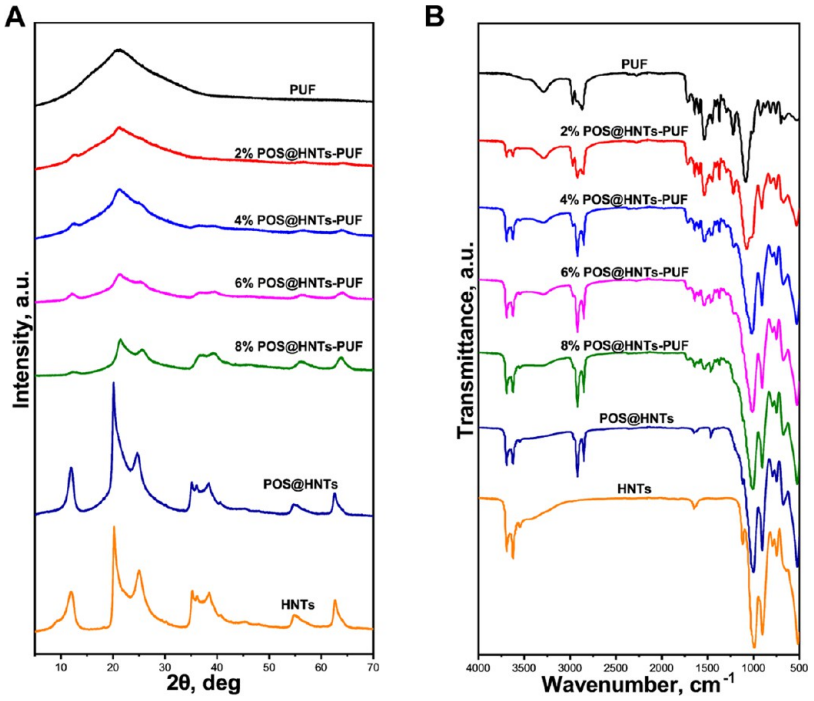

Figure 6. X-ray diffraction patterns (A) and FTIR spectra (B) of pristine HNTs, hydrophobized POS@HNTs, original PUF, and modified POS@HNT-PUF.

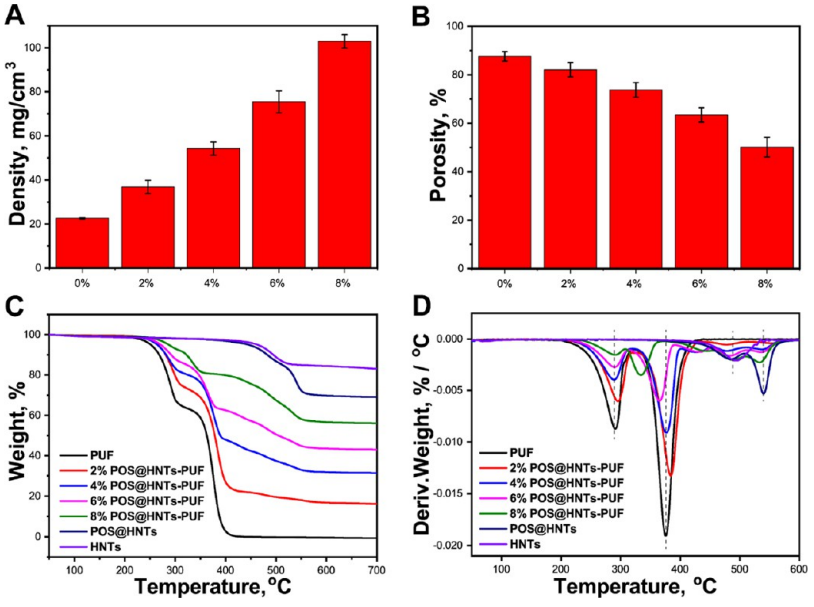

Figure 7. Density (A), porosity (B), thermogravimetric analysis curves (C), and derivative thermogravimetric curve (D) of PUF, POS@HNT-PUF, HNTs, and POS@HNTs.

Raw PUF exhibits a water contact angle of 117 ± 1°, showing some hydrophobicity (Figure 8). However, this is not enough for oil−water separation and water droplets do not readily roll off the surface. Raw halloysite is hydrophilic (contact angle ca. 10°) due to hydroxyl groups on its surface. POS-modified HNTs have greatly enhanced hydrophobicity, and the water contact angle reaches 153 ± 4° (the last photo of Figure 8). After dip coating, the hydrophobicity of POS@HNT-PUF was significantly improved. The higher the content of hydrophobic halloysite, the better the lipophilic properties of the foam. The water contact angles for the four modified PUFs were 139 ± 2, 142 ± 1, 146 ± 1, and 150 ± 3°, respectively.

2.4. Oil Absorption Capacity and Reusability for the Superhydrophobic Foam. The modified foam has a greatly improved oil absorption ability (Supporting Information, Video SV3). POS@HNT-PUF has excellent lipophilic properties and can easily pick up oil droplets below or above the water surface (when the foam was immersed under water by tweezers). The superhydrophobic/superlipophilic foam is quite reflective because of an air bubble layer trapped between the water and the hydrophobic foam. The modified foam has good flexibility, and the oil is easily removed by gently squeezing the

DOI: 10.1021/acsami.9b08023
ACS Appl. Mater. Interfaces 2019, 11, 25445−25456

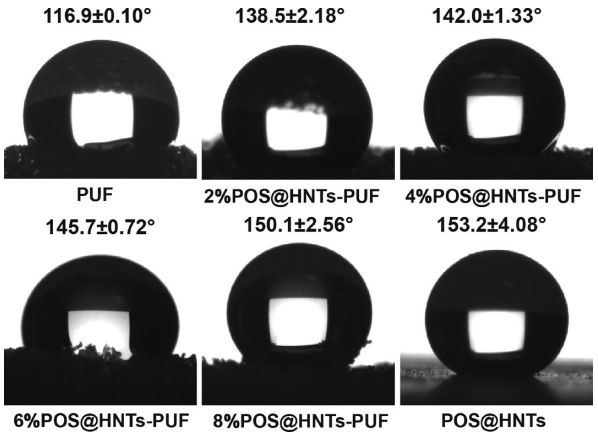

Figure 8. Water contact angle images of PUF, POS@HNT-PUF with 2, 4, 6, 8% POS@HNTs, and hydrophobized POS@HNTs.

foam (Figure 9). Nine different oils and organic solvents were used to evaluate the absorption capacity.

When oil is adsorbed in the hydrophobized foam pores, it fills all of the pore volume and also adsorbed on the outer surface of the foam. The modified foam can absorb 105 times of its own weight in chloroform, although it has different absorption capacities toward different oils and organic agents (Figure 9D). POS@HNT-PUF has higher oil absorption capacity than that of other porous absorbents, such as polydimethylsiloxane sponge, large-pore Fe/C nanocomposite, aerogel, methyltrichlorosilane PUF, MnO_2 nanowires/polyurethane sponge, and poly(dimethylsiloxane)-TiO_2-coated PUF.[16,56−60] This is due to the differences in the oil densities, viscosities, and other properties.[61] For example, the density of chloroform is relatively high, so the modified foam absorbs a larger mass by absorbing the same volume. Methanol is not very dense; therefore, the absorbed mass is less. After the hydrophobic foam was repeatedly used 10 times, the absorption capacity of the foam did not change significantly, which indicates excellent reusability (Figure 9E). However, squeezing the foam does not completely remove all of the oil. After the absorption/desorption cycle, a small fraction of the nanotubes was detached from the foam, but this does not deteriorate the further oil absorption ability (Supporting Information, Figure S3).

A disadvantage of foams for oil−water separation is their limited absorption capacity, which requires a large amount of oil-absorbing foam to be used and transported during the cleaning of large-area oil spills. Connecting the designed hydrophobic foam to a vacuum pump can quickly absorb the oil from the water's surface. To simulate the treatment of oil spills on the sea, we inserted a needle attached to a vacuum into the hydrophobized foam and successfully sucked oil from the surface of the water (Figure 10). After the vacuum pump started, vegetable oil was pulled from the foam into the syringe due to the pressure difference. Vegetable oil was continuously absorbed into the POS@HNT-PUF, making the water's surface clean, and then was drawn into the syringe (Supporting Information, Video SV4). This result illustrates the potential of POS@HNT-PUF for oil/petroleum spill remediation. The technique developed by Cavallaro et al. for internal hydrophobicization of HNTs can be combined with our approach; however, the estimated additional oil absorption will be minor.[62]

2.5. Combustion Performance of the Superhydrophobic Foam. The flame retardancy of the modified PUF was evaluated by an open flame test. Original and modified PUF samples were exposed to a butane torch for 10 s and then monitored until the flame extinguished itself (Figure 11).

When the unmodified original PUF is exposed to flame, it is quickly ignited and generates smoke. It also melts and drips, which could ignite surrounding flammable materials. POS@HNT-PUFs are less flammable, and they will self-extinguish at higher halloysite concentrations.

As the concentration of POS@HNT increases, the integrity of the foam becomes better. In addition, POS@HNT coatings reduce smoke emissions and the modified foams with high halloysite concentrations do not produce melted droplets. The halloysite-coated foam protects against thermal degradation of polyurethane, providing an insulating shield. This prevents the melted polymer from expanding and breaking apart, which could spread the fire. The flame eventually extinguishes itself because there is nothing else flammable on the surface. The engrafted hydroxyl groups of the POS@HNTs dehydrate at high temperatures. This is an endothermic process that releases water vapor to dilute combustible gases and inhibit the release of toxic fumes. This may also be the reason for the excellent flame retardancy. The chemical formula of halloysite is $Al_2Si_2O_5(OH)_4{\cdot}nH_2O$, which consists of multiplexed rolled kaolinite sheets of octahedral gibbsite $Al(OH)_3$ and tetrahedral SiO_4. Metal hydroxides are capable of endothermic decomposition and release of water at high temperatures.[63] In addition, PUF may release a large amount of toxic gases (e.g., CO) during combustion and addition of HNTs can decrease toxic fumes. The combustion residue of POS@HNT-PUF was dissolved in ethanol and analyzed by TEM (Supporting Information, Figure S4). The results show that the main residues of POS@HNT-PUF after combustion are halloysite nanotubes. The tubular structure of the halloysite was retained, and the melted carbonized polyurethane was wrapped around the tubes.

3. CONCLUSIONS

Significantly improved superhydrophobic polymer foam is prepared by dip coating in silanized clay nanotube dispersion (POS@HNTs). SEM, POM, XPS, XRD, and FTIR characterizations indicate that POS@HNTs were successfully prepared and then assembled onto the PUF surface, PUF. The coated hydrophobic PUF shows drastically enhanced lipophilicity, oil absorption, and flame retardancy. POS@HNT-PUF can absorb 105 times of its own weight in chloroform and maintains its absorbency after 10 times of repeated use (soak−squeeze cycles). The modified foam can continuously, effectively, and quickly separate the oil and organic solvents from the water, which has practical significance for oil/water separation. The POS@HNT-coated PUF automatically extinguishes itself and prevents the melted fragments from igniting other flammable materials. Thermally stable POS@HNT-coated foam has a great potential for scaled-up crude oil spills and oil−water separation.

4. EXPERIMENTAL SECTION

4.1. Materials and Reagents. High-purity halloysite (white, powder) was obtained from Guangzhou Runwo Materials Technology Co., Ltd., China. PUF with open-cell structure was purchased from 3M Co. Ltd., China. Hexadecyltrimethoxysilane (HDTMS, ≥85%) was purchased from Aladdin Industrial Co. Ltd., China. Ammonia

DOI: 10.1021/acsami.9b08023
ACS Appl. Mater. Interfaces 2019, 11, 25445−25456

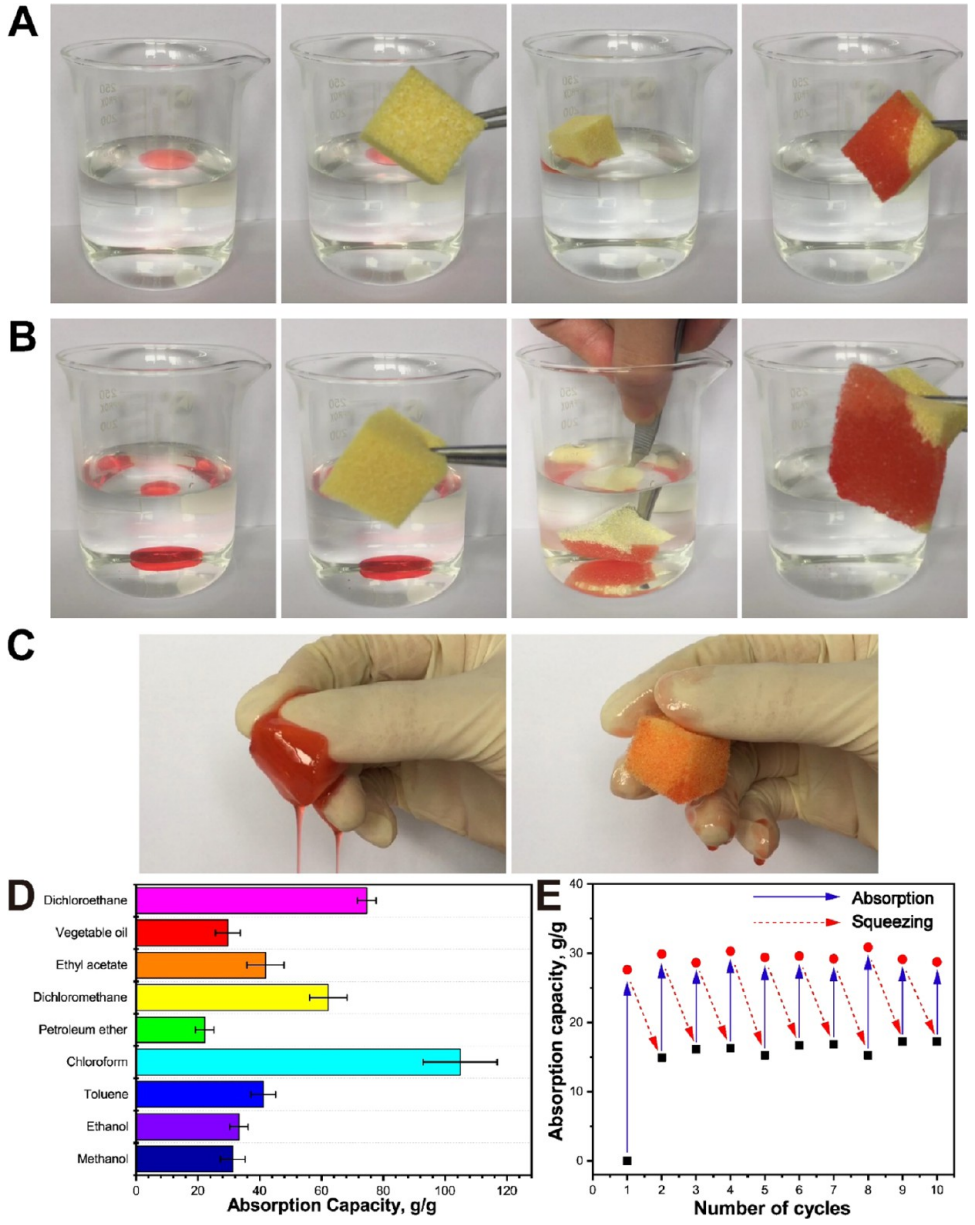

Figure 9. Oil absorption performance of POS@HNT-PUF. Vegetable oil on water surface was removed (A); similarly, chloroform was absorbed from the beaker bottom (B). Recovery of absorbed oil from the foam with finger compression/extrusion (Vegetable oil and chloroform have been colored red for observation) (C). POS@HNT-PUF absorption capacity for different types of oil (D). Cyclic foam absorption-squeezing for vegetable oil (E).

hydroxide was purchased from Guangzhou Chemical Reagent Factory, China. Tetraethoxysilane (TEOS, 98%) and absolute ethanol (density of 0.790 g/mL (20 °C)) were purchased from Tianjin Baishi Chemical Co. Ltd., China. All other chemicals were analytical-grade reagents and used without further purification. Ultrapure DI water was purified by deionization and filtration with a Millipore purification apparatus (resistivity >18.2 MΩ cm).

4.2. Preparation of POS@HNTs. The preparation method of POS@HNTs was similar to the previous work.[42] Typically, 10 g of high-purity HNTs, 5 g of TEOS, and 5 g of HDTMS were sequentially dispersed in a mixture of 200 mL of aqueous ammonia and 40 mL of absolute ethanol. The dispersion was treated with ultrasound at room temperature for 30 min (40 kHz). Next, the hydrolytic condensation was carried out at 60 °C for 30 min and then under magnetic stirring at room temperature for 24 h. After that, the suspension was poured into a glass Petri dish and finally evaporated at room temperature for 24 h to obtain the POS@HNT powder.

4.3. Preparation of POS@HNT Dip-Coated PUF. The technological process of POS@HNT-PUF by dip-coating methods is shown in Figure 1. First, the commercial PUF was washed successively with absolute ethanol using an ultrasonic cleaner (SK1200H, Shanghai Kedao Ultrasonic Instrument Co. Ltd., China) and then dried in a vacuum oven (DZF-6051, Shanghai Yiheng Scientific Instruments Co. Ltd., China) at 100 °C for several hours. Subsequently, POS@HNTs were dispersed in absolute ethanol under ultrasonic treatment at 40 kHz for 30 min with different concentrations of 2, 4, 6, and 8% (weight percent). After that, the dried PUF was immersed in the suspension of POS@HNTs and repeatedly squeezed until no bubbles were produced. Finally, the foams were dried in the vacuum oven at 100 °C for 2 h. The PUF was turned over every half hour to ensure a uniform coating of POS@HNTs.

4.4. Characterization. *4.4.1. Hydrophobic Halloysite Marble Formation.* The marble was made by rolling a droplet on the surface

DOI: 10.1021/acsami.9b08023
ACS Appl. Mater. Interfaces 2019, 11, 25445−25456

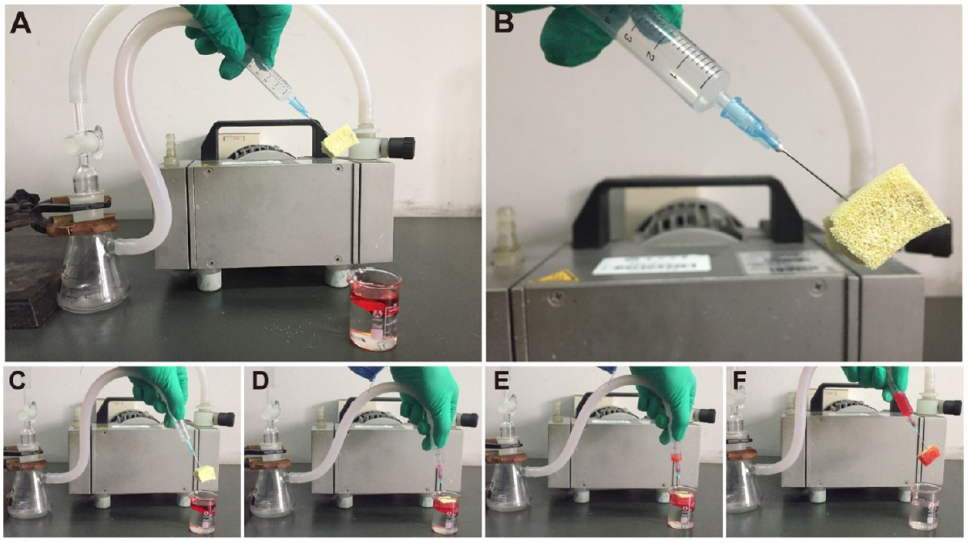

Figure 10. Vacuum device for separating oil and water with hydrophobic HNT-coated PUF as a separator (A, B). Images of the continuous separation of red-colored vegetable oil from the water surface using a collection device (C−F).

Figure 11. Torch burn test of origianl PUF (0%) and differnt-content POS@HNT-PUF. Before exposure to the torch flame (A), after exposure for 5 s (B), after removal of the torch (C), 5 s later (D), and self-extinguishing after 30 s (E).

of POS@HNTs. The volume of the droplets was controlled at 20 μL by a pipette.

4.4.2. Polarized Optical Microscope (POM). PUF and POS@HNT-PUF with the thickness of 1 mm were placed on glass plates and photographed using a POM (BX51, Olympus Corporation, Japan).

4.4.3. Scanning Electron Microscope (SEM). The open-cell structures of PUF and POS@HNT-PUF were observed by a tabletop SEM (TM3030, Hitachi Ltd., Japan) at 15 kV. Before observation, the samples were coated with gold using a sputtering coater.

4.4.4. X-ray Photoelectron Spectrum (XPS). The X-ray photoelectron spectroscopy analyses were determined by an XPS instrument (K-Alpha$^+$, Thermo Fisher Scientific Co. Ltd.) with Al Kα radiation. The atoms of N, C, O, Al, and Si were detected.

4.4.5. Fourier Transform Infrared (FTIR) Spectroscopy. The FTIR spectra were measured using attenuated total reflectance by a Thermo FTIR (Nicolet iS50, Thermo Fisher Scientific Co. Ltd.). The scans were performed 32 times in succession, and their average values were saved. The spectra were taken at 4000−500 cm^{-1}. The wavenumber resolution was 2 cm^{-1}.

4.4.6. X-ray Diffraction (XRD). The XRD patterns were obtained using an XRD machine (Miniflex 600, Rigaku Corporation, Japan) at an acceleration voltage of 40 kV and a current of 40 mA with a scanning rate of 5°/min.

4.4.7. Density. The densities of PUF and POS@HNT-PUF were determined by measuring weight and volume of each individual foam. The weight of the samples was measured by an analytical balance (readable 0.0001 g, ME204E, Mettler Toledo Co. Ltd., Switzerland), and the size of the samples was measured by a digital caliper. Five samples were used for density determination for each group. The density was calculated by the following equation.

DOI: 10.1021/acsami.9b08023
ACS Appl. Mater. Interfaces 2019, 11, 25445−25456

$$\text{density} = \frac{m}{lwh} \quad (1)$$

where m, l, w, and h are the weight, length, width, and height of the samples, respectively.

4.4.8. Porosity. The porosites of PUF and POS@HNT-PUF were measured by the following procedure. First, the size and weight of the samples were measured and recorded, respectively. Samples of different POS@HNT contents were then immersed in absolute ethanol for 24 h at room temperature. Finally, we gently sample and measure the weight of the samples after soaking. Five samples were used for porosity determination for each group. The porosity was calculated by the following equation.

$$\text{porosity} = \frac{m_a - m}{\rho lwh} \times 100\% \quad (2)$$

where m_a is the weight of the samples after soaking in absolute ethanol. ρ is the density of absolute ethanol. m, l, w, and h are the weight, length, width, and height of the dry samples, respectively.

4.4.9. Mechanical Property Test. The compressive stress−strain curves were measured using a universal testing machine (UTM-Q422, Chengde Jinjian Testing Instrument Co. Ltd., China). The samples used for the test were a cuboid sample with the side length of 10 mm.

4.4.10. Thermogravimetric Analyzer (TGA). The TGA curves were tested using the TGA (TGA2, Mettler Toledo Co. Ltd., Switzerland) under a nitrogen atmosphere from 50 to 700 °C at a heating rate of 10 °C/min.

4.4.11. Water Contact Angle. The surface hydrophilicity was determined using a drop-shape analyzer (DSA100, Kruss Co. Ltd., Germany) at room temperature. The contact angles were measured just after the liquid deposition onto the substrate. Liquid droplet volume was 5.0 ± 0.5 μL. At least, five measurements were carried out on each sample.

4.4.12. Absorption Test. Oil and organic solvent were added dropwise to the beaker. Then, the preweighed POS@HNT-PUF was immersed in the solvents to be fully absorbed. Once the saturated foam was removed from the beaker, the weight of the foam was weighed immediately. Finally, the foam was repeatedly squeezed to remove most of the solvents absorbed. Each sample was measured at least 3 times and averaged. The absorption capacity was calculated by the following equation.

$$\text{absorptioncapacity} = \frac{m_b - m}{m} \quad (3)$$

where m_b is the weight of the samples after soaking in the solvents and m is the weight of the dry samples.

4.4.13. Cyclic Absorption Test. The reusability of POS@HNT-PUF was evaluated by mechanical squeezing. First, the weight of the dry foam was measured and recorded. Next, the foam was immersed in the liquid for maximum absorption and the weight of the foam was measured. The absorbed liquid was then removed by a simple finger squeeze. After that, the weight of the foam was again measured and recorded. A total of 10 absorption−squeezing cycles were performed.

4.4.14. Continuous Absorption Test. The continuous absorption system consists of POS@HNT-PUF, vacuum pump, syringe, flask, and some rubber tubes. The needle of the syringe was inserted into the interior of the foam, and the foam was immersed in the oil−water mixture. One end of the rubber tube was connected to the syringe, and the other end of the rubber tube was connected to the flask. In the oil test from the water, the vacuum pump was turned on and the oil was continuously removed from the water surface by the superhydrophobicity of the foam. The power of the entire process was provided by a vacuum pump.

4.4.15. Torch Burn Test. The qualitative assessment of foam flammability was exposure to direct flame from butane torch for 10 s. The blue flame showed butane flame temperature of about 1300 °C. The combustion behavior of the samples (such as flame spreading, dropping, carbonization, and flame separation) was visually evaluated, and the photo was recorded.

4.4.16. Transmission Electron Microscopy (TEM). The morphologies were observed by TEM (JEM-2100F, JEOL Co. Ltd., Japan) under an accelerating voltage of 100 kV. The samples were dispersed in absolute ethanol or ultrapure DI water by ultrasound and dripped onto a copper mesh before observation.

■ ASSOCIATED CONTENT

Supporting Information

The Supporting Information is available free of charge on the ACS Publications website at DOI: 10.1021/acsami.9b08023.

Water contact angle image of HDTMS@HNTs; SEM image of POS@HNT-PUF after absorption/desorption cycles; compressive stress−strain curves of PUF and 8% POS@HNT-PUF; TEM images of POS@HNT-PUF, after the torch burn test (PDF)

Movement of hydrophobic halloysite marble (Video SV1) (AVI)

Hydrophobic performance of PUF and POS@HNT-PUF (Video SV2) (AVI)

Oil absorption ability of POS@HNT-PUF (Video SV3) (AVI)

Continuous absorption behavior of POS@HNT-PUF (Video SV4) (AVI)

■ AUTHOR INFORMATION

Corresponding Authors

*E-mail: liumx@jnu.edu.cn (M.L.).
*E-mail: ylvov@latech.edu (Y.L.).

ORCID

Mingxian Liu: 0000-0002-5466-3024
Yuri Lvov: 0000-0003-0722-5643

Notes

The authors declare no competing financial interest.

■ ACKNOWLEDGMENTS

This work was financially supported by the National Natural Science Foundation of China (51473069 and 51502113), the Pearl River S&T Nova Program of Guangzhou (201610010026), and the Fundamental Research Funds for the Central Universities (21619102). Y.L. thanks support by act 211 of the Russian Federation, # 02.A03.21.0006.

■ REFERENCES

(1) Carpenter, A. Oil pollution in the North Sea: the Impact of Governance Measures on Oil Pollution Over Several Decades. *Hydrobiologia* **2018**, 1−19.

(2) Joye, S. B. Deepwater Horizon, 5 Years on. *Science* **2015**, *349*, 592−593.

(3) Bhardwaj, N.; Bhaskarwar, A. N. A Review on Sorbent Devices for Oil-Spill Control. *Environ. Pollut.* **2018**, *243*, 1758−1771.

(4) Nyankson, E.; Rodene, D.; Gupta, R. B. Advancements in Crude Oil Spill Remediation Research After the Deepwater Horizon Oil Spill. *Water, Air, Soil Pollut.* **2016**, *227*, 29.

(5) Fox, C. H.; O'Hara, P.; Bertazzon, S.; Morgan, K.; Underwood, F. E.; Paquet, P. A Preliminary Spatial Assessment of Risk: Marine Birds and Chronic Oil Pollution on Canada's Pacific Coast. *Sci. Total Environ.* **2016**, *573*, 799−809.

(6) Ivshina, I. B.; Kuyukina, M. S.; Krivoruchko, A. V.; Elkin, A. A.; Makarov, S. O.; Cunningham, C. J.; Peshkur, T. A.; Atlas, R. M.; Philp, J. C. Oil Spill Problems and Sustainable Response Strategies Through New Technologies. *Environ. Sci.: Processes Impacts* **2015**, *17*, 1201−1219.

DOI: 10.1021/acsami.9b08023
ACS Appl. Mater. Interfaces 2019, 11, 25445−25456

(7) Prendergast, D. P.; Gschwend, P. M. Assessing the Performance and Cost of Oil Spill Remediation Technologies. *J. Cleaner Prod.* **2014**, *78*, 233−242.
(8) Sarbatly, R.; Krishnaiah, D.; Kamin, Z. A Review of Polymer Nanofibres by Electrospinning and Their Application in Oil−Water Separation for Cleaning up Marine Oil Spills. *Mar. Pollut. Bull.* **2016**, *106*, 8−16.
(9) Zhang, Y.; He, X.; Ouyang, J.; Yang, H. Palladium Nanoparticles Deposited on Silanized Halloysite Nanotubes: Synthesis, Characterization and Enhanced Catalytic Property. *Sci. Rep.* **2013**, *3*, No. 2948.
(10) Saleem, J.; Riaz, M. A.; Gordon, M. Oil Sorbents from Plastic Wastes and Polymers: A review. *J. Hazard. Mater.* **2018**, *341*, 424−437.
(11) Zeng, X.; Xu, S.; Pi, P.; Cheng, J.; Wang, L.; Wang, S.; Wen, X. Polymer-Infiltrated Approach to Produce Robust and Easy Repairable Superhydrophobic Mesh for High-Efficiency Oil/Water Separation. *J. Mater. Sci.* **2018**, *53*, 10554−10568.
(12) Li, S.; Huang, J.; Ge, M.; Cao, C.; Deng, S.; Zhang, S.; Chen, G.; Zhang, K.; Al-Deyab, S. S.; Lai, Y. Robust Flower-Like TiO_2@ Cotton Fabrics with Special Wettability for Effective Self-Cleaning and Versatile Oil/Water Separation. *Adv. Mater. Interfaces* **2015**, *2*, No. 1500220.
(13) Tjandra, R.; Lui, G.; Veilleux, A.; Broughton, J.; Chiu, G.; Yu, A. Introduction of an Enhanced Binding of Reduced Graphene Oxide to Polyurethane Sponge for Oil Absorption. *Ind. Eng. Chem. Res.* **2015**, *54*, 3657−3663.
(14) Wang, X.; Pan, Y.; Liu, X.; Liu, H.; Li, N.; Liu, C.; Schubert, D. W.; Shen, C. Facile Fabrication of Superhydrophobic and Eco-Friendly Polylactic Acid Foam for Oil-Water Separation via Skin-Peeling. *ACS Appl. Mater. Interfaces* **2019**, 14362−14367.
(15) Bu, X.; Lu, Y.; Chen, S.; Li, D.; Zhang, Z.; Qian, P. Fabrication of Porous Carbon Nitride Foams/Acrylic Resin Composites for Efficient Oil and Organic Solvents Capture. *Chem. Eng. J.* **2019**, *355*, 299−308.
(16) Zhang, T.; Kong, L.; Dai, Y.; Yue, X.; Rong, J.; Qiu, F.; Pan, J. Enhanced Oils and Organic Solvents Absorption by Polyurethane Foams Composites Modified with MnO_2 Nanowires. *Chem. Eng. J.* **2017**, *309*, 7−14.
(17) Cao, Z.-J.; Dong, X.; Fu, T.; Deng, S.-B.; Liao, W.; Wang, Y.-Z. Coated vs. Naked Red Phosphorus: A Comparative Study on their Fire Retardancy and Smoke Suppression for Rigid Polyurethane Foams. *Polym. Degrad. Stab.* **2017**, *136*, 103−111.
(18) Liu, Y.; Ma, J.; Wu, T.; Wang, X.; Huang, G.; Liu, Y.; Qiu, H.; Li, Y.; Wang, W.; Gao, J. Cost-Effective Reduced Graphene Oxide-Coated Polyurethane Sponge as a Highly Efficient and Reusable Oil-Absorbent. *ACS Appl. Mater. Interfaces* **2013**, *5*, 10018−10026.
(19) Nikkhah, A. A.; Zilouei, H.; Asadinezhad, A.; Keshavarz, A. Removal of Oil from Water Using Polyurethane Foam Modified with Nanoclay. *Chem. Eng. J.* **2015**, *262*, 278−285.
(20) Ruan, C.; Ai, K.; Li, X.; Lu, L. A Superhydrophobic Sponge with Excellent Absorbency and Flame Retardancy. *Angew. Chem., Int. Ed.* **2014**, *53*, 5556−5560.
(21) Kim, H.; Kim, D. W.; Vasagar, V.; Ha, H.; Nazarenko, S.; Ellison, C. J. Polydopamine-Graphene Oxide Flame Retardant Nanocoatings Applied via an Aqueous Liquid Crystalline Scaffold. *Adv. Funct. Mater.* **2018**, *28*, No. 1803172.
(22) Zhou, X.; Zhang, Z.; Xu, X.; Men, X.; Zhu, X. Facile Fabrication of Superhydrophobic Sponge with Selective Absorption and Collection of Oil from Water. *Ind. Eng. Chem. Res.* **2013**, *52*, 9411−9416.
(23) Wu, L.; Li, L.; Li, B.; Zhang, J.; Wang, A. Magnetic, Durable, and Superhydrophobic Polyurethane@ Fe3O4@ SiO2@ Fluoropolymer Sponges for Selective Oil Absorption and Oil/Water Separation. *ACS Appl. Mater. Interfaces* **2015**, *7*, 4936−4946.
(24) Li, C.; Sun, Y.; Cheng, M.; Sun, S.; Hu, S. Fabrication and Characterization of a TiO2/Polysiloxane Resin Composite Coating with Full-Thickness Super-Hydrophobicity. *Chem. Eng. J* **2018**, *333*, 361−369.
(25) Shaker, M.; Salahinejad, E. A Combined Criterion of Surface Free Energy and Roughness to Predict the Wettability of Non-Ideal Low-Energy Surfaces. *Prog. Org. Coat* **2018**, *119*, 123−126.
(26) Mi, H.-Y.; Jing, X.; Xie, H.; Huang, H.-X.; Turng, L.-S. Magnetically Driven Superhydrophobic Silica Sponge Decorated with Hierarchical Cobalt Nanoparticles for Selective Oil Absorption and Oil/Water Separation. *Chem. Eng. J* **2018**, *337*, 541−551.
(27) Qiu, S.; Li, Y.; Li, G.; Zhang, Z.; Li, Y.; Wu, T. Robust Superhydrophobic Sepiolite-Coated Polyurethane Sponge for Highly Efficient and Recyclable Oil Absorption. *ACS Sustainable Chem. Eng.* **2019**, *7*, 5560−5567.
(28) Wei, Q.; Oribayo, O.; Feng, X.; Rempel, G. L.; Pan, Q. Synthesis of Polyurethane Foams Loaded with TiO2 Nanoparticles and their Modification for Enhanced Performance in Oil Spill Cleanup. *Ind. Eng. Chem. Res.* **2018**, *57*, 8918−8926.
(29) Cavallaro, G.; Lazzara, G.; Milioto, S.; Parisi, F. Hydrophobically Modified Halloysite Nanotubes as Reverse Micelles for Water-in-Oil Emulsion. *Langmuir* **2015**, *31*, 7472−7478.
(30) Liu, M.; Fakhrullin, R.; Novikov, A.; Panchal, A.; Lvov, Y. Tubule Nanoclay-Organic Heterostructures for Biomedical Applications. *Macromol. Biosci.* **2018**, No. 1800419.
(31) Lazzara, G.; Cavallaro, G.; Panchal, A.; Fakhrullin, R.; Stavitskaya, A.; Vinokurov, V.; Lvov, Y. An Assembly of Organic-Inorganic Composites Using Halloysite Clay Nanotubes. *Curr. Opin. Colloid Interface Sci.* **2018**, *35*, 42−50.
(32) Zhang, H.; Cheng, C.; Song, H.; Bai, L.; Cheng, Y.; Ba, X.; Wu, Y. A Facile One-Step Grafting of Polyphosphonium onto Halloysite Nanotubes Initiated by Ce(iv). *Chem. Commun.* **2019**, *55*, 1040−1043.
(33) Lvov, Y.; Wang, W.; Zhang, L.; Fakhrullin, R. Halloysite Clay Nanotubes for Loading and Sustained Release of Functional Compounds. *Adv. Mater.* **2016**, *28*, 1227−1250.
(34) Wu, F.; Zheng, J.; Li, Z.; Liu, M. Halloysite Nanotubes Coated 3D Printed PLA Pattern for Guiding Human Mesenchymal Stem Cells (HMSCs) Orientation. *Chem. Eng. J.* **2019**, *359*, 672−683.
(35) Smith, R. J.; Holder, K. M.; Ruiz, S.; Hahn, W.; Song, Y.; Lvov, Y. M.; Grunlan, J. C. Environmentally Benign Halloysite Nanotube Multilayer Assembly Significantly Reduces Polyurethane Flammability. *Adv. Funct. Mater.* **2018**, *28*, No. 1703289.
(36) Buruga, K.; Kalathi, J. T. A Facile Synthesis of Halloysite Nanotubes Based Polymer Nanocomposites for Glass Coating Application. *J. Alloys Compd.* **2018**, *735*, 1807−1817.
(37) Lvov, Y. M.; Shchukin, D. G.; Möhwald, H.; Price, R. R. Halloysite Clay Nanotubes for Controlled Release of Protective Agents. *ACS Nano* **2008**, *2*, 814−820.
(38) Baidya, A.; Ganayee, M. A.; Jakka Ravindran, S.; Tam, K. C.; Das, S. K.; Ras, R. H.; Pradeep, T. Organic Solvent-Free Fabrication of Durable and Multifunctional Superhydrophobic Paper from Waterborne Fluorinated Cellulose Nanofiber Building Blocks. *ACS Nano* **2017**, *11*, 11091−11099.
(39) Zhou, H.; Wang, H.; Niu, H.; Lin, T. Recent Progress in Durable and Self-Healing Super-Nonwettable Fabrics. *Adv. Mater. Interfaces* **2018**, *5*, No. 1800461.
(40) Chen, D.; Gao, H.; Jin, Z.; Wang, J.; Dong, W.; Huang, X.; Wang, G. Vacuum-Dried Synthesis of Low-Density Hydrophobic Monolithic Bridged Silsesquioxane Aerogels for Oil/Water Separation: Effects of Acid Catalyst and Its Excellent Flexibility. *ACS Appl. Nano Mater.* **2018**, *1*, 933−939.
(41) Schmidt, H.; Scholze, H.; Kaiser, A. Principles of Hydrolysis and Condensation Reaction of Alkoxysilanes. *J. Non-Cryst. Solids* **1984**, *63*, 1−11.
(42) Feng, K.; Hung, G.-Y.; Liu, J.; Li, M.; Zhou, C.; Liu, M. Fabrication of High Performance Superhydrophobic Coatings by Spray-Coating of Polysiloxane Modified Halloysite Nanotubes. *Chem. Eng. J.* **2018**, *331*, 744−754.
(43) Zhang, Y.; Zhang, J.; Wang, A. From Maya Blue to Biomimetic Pigments: Durable Biomimetic Pigments with Self-Cleaning Property. *J. Mater. Chem. A* **2016**, *4*, 901−907.

DOI: 10.1021/acsami.9b08023
ACS Appl. Mater. Interfaces 2019, 11, 25445−25456

(44) Panchal, A.; Fakhrullina, G.; Fakhrullin, R.; Lvov, Y. Self-Assembly of Clay Nanotubes on Hair Surface for Medical and Cosmetic Formulations. *Nanoscale* **2018**, *10*, 18205−18216.
(45) Xue, Z.; Cao, Y.; Liu, N.; Feng, L.; Jiang, L. Special Wettable Materials for Oil/Water Separation. *J. Mater. Chem. A* **2014**, *2*, 2445−2460.
(46) Chu, Z.; Feng, Y.; Seeger, S. Oil/Water Separation with Selective Superantiwetting/Superwetting Surface Materials. *Angew. Chem., Int. Ed.* **2015**, *54*, 2328−2338.
(47) Ma, Q.; Cheng, H.; Fane, A. G.; Wang, R.; Zhang, H. Recent Development of Advanced Materials with Special Wettability for Selective Oil/Water Separation. *Small* **2016**, *12*, 2186−2202.
(48) Luo, L.; Chen, X.; Wang, Y.; Yue, J.; Du, Z.; Huang, X.; Tang, X.-Z. Bio-Inspired Modification of Silicon Carbide Foams for Oil/Water Separation and Rapid Power-Free Absorption towards Highly Viscous Oils. *Ceram. Int.* **2018**, *44*, 12021−12029.
(49) Guo, D.; Chen, J.; Hou, K.; Xu, S.; Cheng, J.; Wen, X.; Wang, S.; Huang, C.; Pi, P. A Facile Preparation of Superhydrophobic Halloysite-Based Meshes for Efficient Oil−Water Separation. *Appl. Clay Sci.* **2018**, *156*, 195−201.
(50) Zia, K. M.; Bhatti, I. A.; Barikani, M.; Zuber, M.; Sheikh, M. A. XRD Studies of Chitin-Based Polyurethane Elastomers. *Int. J. Biol. Macromol.* **2008**, *43*, 136−141.
(51) Ledoux, R. L.; White, J. L. Infrared Study of the OH Groups in Expanded Kaolinite. *Science* **1964**, *143*, 244−246.
(52) Szczepanik, B.; Słomkiewicz, P.; Garnuszek, M.; Czech, K.; Banaś, D.; Kubala-Kukuś, A.; Stabrawa, I. The Effect of Chemical Modification on the Physico-Chemical Characteristics of Halloysite: FTIR, XRF, and XRD Studies. *J. Mol. Struct.* **2015**, *1084*, 16−22.
(53) Pinto, J.; Athanassiou, A.; Fragouli, D. Effect of the Porous Structure of Polymer Foams on the Remediation of Oil Spills. *J. Phys. D: Appl. Phys.* **2016**, *49*, No. 145601.
(54) Gorrasi, G.; Bugatti, V.; Ussia, M.; Mendichi, R.; Zampino, D.; Puglisi, C.; Carroccio, S. C. Halloysite Nanotubes and Thymol as Photo Protectors of Biobased Polyamide 11. *Polym. Degrad. Stab.* **2018**, *152*, 43−51.
(55) Therias, S.; Murariu, M.; Dubois, P. Bionanocomposites Based on PLA and Halloysite Nanotubes: From Key Properties to Photooxidative Degradation. *Polym. Degrad. Stab.* **2017**, *145*, 60−69.
(56) Choi, S.-J.; Kwon, T.-H.; Im, H.; Moon, D.-I.; Baek, D. J.; Seol, M.-L.; Duarte, J. P.; Choi, Y.-K. A Polydimethylsiloxane (PDMS) Sponge for the Selective Absorption of Oil from Water. *ACS Appl. Mater. Interfaces* **2011**, *3*, 4552−4556.
(57) Chu, Y.; Pan, Q. Three-Dimensionally Macroporous Fe/C Nanocomposites as Highly Selective Oil-Absorption Materials. *ACS Appl. Mater. Interfaces* **2012**, *4*, 2420−2425.
(58) Du, R.; Zhang, N.; Xu, H.; Mao, N.; Duan, W.; Wang, J.; Zhao, Q.; Liu, Z.; Zhang, J. CMP Aerogels: Ultrahigh-Surface-Area Carbon-Based Monolithic Materials with Superb Sorption Performance. *Adv. Mater.* **2014**, *26*, 8053−8058.
(59) Zhu, Q.; Chu, Y.; Wang, Z.; Chen, N.; Lin, L.; Liu, F.; Pan, Q. Robust Superhydrophobic Polyurethane Sponge as a Highly Reusable Oil-Absorption Material. *J. Mater. Chem. A* **2013**, *1*, 5386−5393.
(60) Shuai, Q.; Yang, X.; Luo, Y.; Tang, H.; Luo, X.; Tan, Y.; Ma, M. A Superhydrophobic Poly (dimethylsiloxane)-TiO2 Coated Polyurethane Sponge for Selective Absorption of Oil from Water. *Mater. Chem. Phys.* **2015**, *162*, 94−99.
(61) Wang, X.; Lu, Y.; Carmalt, C. J.; Parkin, I. P.; Zhang, X. Multifunctional Porous and Magnetic Silicone with High Elasticity, Durability, and Oil−Water Separation Properties. *Langmuir* **2018**, *34*, 13305−13311.
(62) Cavallaro, G.; Grillo, I.; Gradzielski, M.; Lazzara, G. Structure of Hybrid Materials Based on Halloysite Nanotubes Filled with Anionic Surfactants. *J. Phys. Chem. C* **2016**, *120*, 13492−13502.
(63) Laoutid, F.; Bonnaud, L.; Alexandre, M.; Lopez-Cuesta, J. M.; Dubois, P. New Prospects in Flame Retardant Polymer Materials: From Fundamentals to Nanocomposites. *Mater. Sci. Eng., R* **2009**, *63*, 100−125.

DOI: 10.1021/acsami.9b08023
ACS Appl. Mater. Interfaces 2019, 11, 25445−25456